Phosphorescent Cationic Iridium(III) Complexes Bearing a Nonconjugated Six-Membered Chelating Ancillary Ligand: A Strategy for Tuning the Emission Towards the Blue

Claus Hierlinger,[a,b] *David B. Cordes,*[b] *Alexandra M. Z. Slawin,*[b] *Denis Jacquemin**[c]

*Véronique Guerchais**[a] *Eli Zysman-Colman**[b]

[a] Univ Rennes, CNRS, ISCR (Institut des Sciences Chimiques de Rennes) – UMR 6226, F-35000 Rennes, France. E-mail: veronique.guerchais@univ-rennes1.fr

[b] Organic Semiconductor Centre, EaStCHEM School of Chemistry, University of St Andrews, St Andrews, Fife, KY16 9ST, UK. E-mail : eli.zysman-colman@st-andrews.ac.uk; Web: http://www.zysman-colman.com

[c] UMR CNRS 6230, Université de Nantes, CEISAM, 2 rue de la Houssinière, 44322 Nantes Cedex 3, France. E-mail: Denis.Jacquemin@univ-nantes.fr

Abstract

This study concerns an assessment of the impact of the interruption of the electronic crosstalk between the pyridine rings in the ancillary ligand on the photoluminescence properties of the corresponding iridium(III) complexes. Two new cationic Ir(III) complexes, $[Ir(dFmesppy)_2(pmdp)]PF_6$, **1**, and $[Ir(mesppy)_2(pmdp)]PF_6$, **2**, [where dFmesppy is 2-(2,4-difluorophenyl)-4-mesitylpyridinato, mesppy is 4-mesityl-2-phenylpyridinato and pmdp is 2,2'-(phenylmethine)dipyridine, **L1**] possessing sterically congested cyclometalating ligands combined with the nonconjugated diimine ancillary N^N ligand are reported and their solution-state and thin film photophysical properties analyzed by both experimental and theoretical methods. The crystal structure of **1** confirms the formation of a six-membered chelate ring by the N^N ligand and illustrates the pseudo-axial configuration of the phenyl substituents. Upon photoexcitation in acetonitrile, both complexes exhibit a ligand-centered emission profile in the blue-green region of the visible spectrum. A significant blue-shift is observed in solution at room temperature compared to the analogous reference Ir(III) complexes (**R1** and **R2**) bearing 4,4'-di-*tert*-butyl-2,2'-bipyridine (d*t*Bubpy) as the N^N ligand. The computational investigation demonstrates that the HOMO is mainly centered on the metal and on both cyclometalating aryl rings of the C^N ligands, whereas the LUMO is principally localized on the pyridyl rings of the C^N ligands. The photoluminescence quantum yield is reduced compared to the reference complexes, a probable consequence of the greater flexibility of the ancillary ligand.

Introduction

Iridium(III) complexes are attractive phosphors because of their generally high photoluminescence quantum yields, Φ_{PL}, their relatively short emission state lifetimes, τ_{PL}, and their facile and wide emission color tunability as a function of ligand identity.[1] In

electroluminescent devices such as organic light emitting diodes (OLEDs)[2] and light-emitting electrochemical cells (LEECs),[3] blue emissive materials are critical components for full-color displays and for the generation of white light in the context of solid-state lighting.[4] Charged complexes are particularly germane for LEECs. Typically, heteroleptic cationic Ir(III) complexes of the form $[Ir(C^N)_2(N^N)]^+$ consist of two cyclometalating C^N ligands, often based on a 2-phenylpyridinato (ppy) scaffold, and one five-membered chelating diimine N^N ancillary ligand such as 2,2'-bipyridine (bpy), 1,10-phenanthroline (phen) or their derivatives. The emission energy is normally tuned through substituent decoration about these ligands, with typically electron-withdrawing groups attached to the C^N ligands and electron-donating groups incorporated onto the N^N ligand. These changes in electronic properties of the different ligands are used in concert to increase the HOMO-LUMO gap, and by extension the energy of the emissive triplet state. Much less attention has been devoted to the impact of changing the chelate ring size of either ligand type on the emission energy, particularly in the context of the incorporation of an sp^3 carbon spacer between the coordinating rings, breaking their conjugation. Bidentate chelating C^N ligands forming six-membered rings remain rare and can be assigned into one of two categories, whether they contain conjugated[5] or nonconjugated[6] chelating ligands. Recently, we reported[7] a series of tripodal C^N^C ligands based on 2-benzhydrylpyridine that can form three six-membered chelate rings through a double C-H bond activation when coordinated to the iridium center. We also investigated the impact of a conformationally flexible C^N ligand within a family of $[Ir(bnpy)(N^N)]PF_6$ complexes; employing the nonconjugated six-membered chelating benzylpyridinato (bnpy) as the C^N ligand.[8] Depending on the nature of the N^N ligand, we observed phosphorescence ranging from yellow to red and marked variations of the ratio of the conformers.

The use of six-membered chelate ancillary ligands on cationic iridium(III) complexes is more common though there are only a handful of reports for this category as well (Chart **1**). Examples include the use of a di(pyridin-2-yl)methane (dpm) that incorporates a methylene spacer to interrupt the π-conjugation[9] of the ligand such as $[Ir(ppy)_2(dpm)]PF_6$; unfortunately, no photophysics was reported for this complex. Other studies have focused on the functionalization of this methylene bridge. For instance, the complexes $[Ir(ppy)_2(dpyOH\text{-}R)]Cl$ [where R = H and CH_2CN, giving dpyOH-R as di(pyridin-2-yl)methanol and 3-hydroxy-3,3-di(pyridine-2-yl)propanenitrile, respectively] have been investigated.[10] The effect of successfully interrupting the direct electronic crosstalk between the coordination moieties was demonstrated by comparing the photophysical properties of $[Ir(ppy)_2(dpyOH)]Cl$ (with λ_{PL} = 477, 507 and 547 nm, Φ_{PL} = 10% in MeCN) and the reference complex $[Ir(ppy)_2(bpy)]PF_6$ (λ_{PL} = 602 nm, Φ_{PL} = 9% in MeCN);[11] a large blue-shift of 125 nm (4353 cm^{-1}) was indeed observed. The complex $[Ir(ppy)_2(dpyOH\text{-}CH_2CN)]Cl$ (with λ_{PL} = 535 nm, Φ_{PL} = 49% in MeCN) is surprisingly a brighter emitter than the structurally related complexes shown in Chart **1**, exhibiting predominantly MLCT emission. The two complexes $[Ir(ppy)_2(dpy\text{-}R)]Cl$ [where R = O and $N\text{-}NH_2$, giving dpy-R as di-2-pyridylketone and 2,2'-(hydrazonomethylene)dipyridine, respectively] are very poor emitters in acetonitrile, with $\Phi_{PL} < 0.5\%$. The former exhibits an unstructured emission centered at 678 nm, whereas the latter displays a blue-shifted, structured emission profile (λ_{PL} = 480, 510 nm).[10]

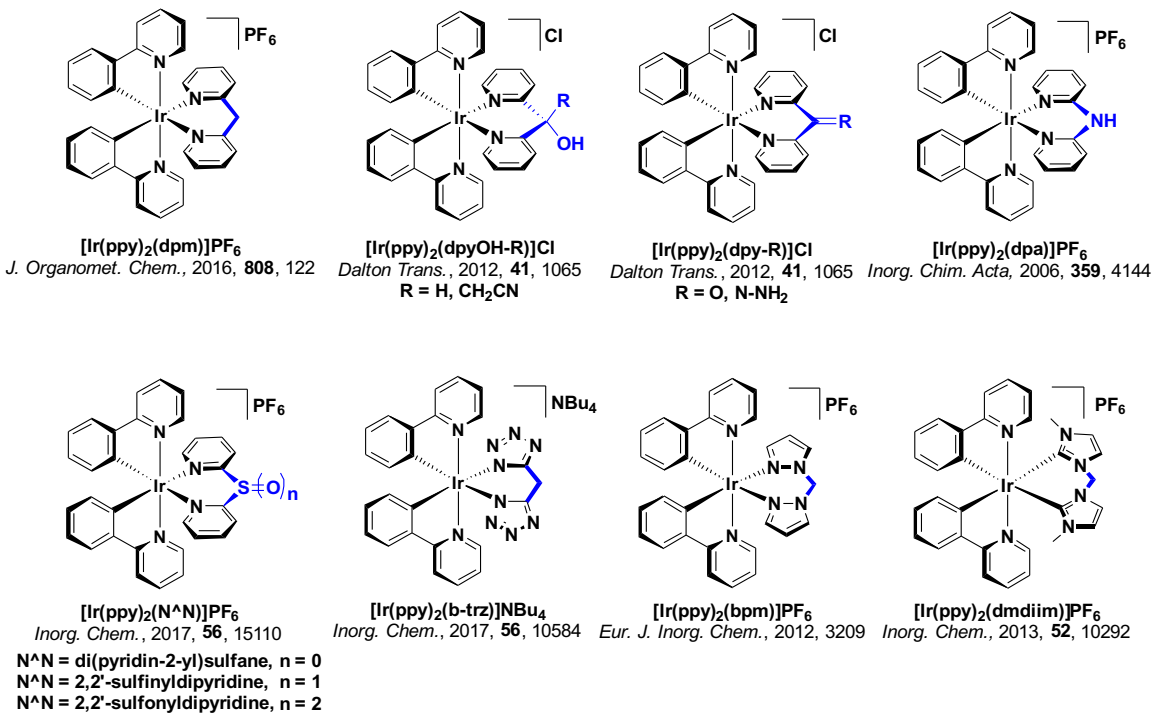

Chart **1**. Structural representation of Iridium(III) complexes bearing conjugated and nonconjugated six-membered chelate ancillary ligands reported in the literature.

A more widely studied six-membered chelate N^N ligand is di(pyridin-2-yl)amine (dpa).[9, 12] With $[Ir(ppy)_2(dpa)]PF_6$ [λ_{PL} = 483, 514 (sh) nm, Φ_{PL} = 43% in CH_2Cl_2] a significant blue-shift and increase in Φ_{PL} can be observed with respect to $[Ir(ppy)_2(bpy)]PF_6$, which is a result of the presence of the electron-donating central amine.[12a] Using sulfur-bridged six-membered chelate N^N ligands [di(pyridine-2-yl)sulfane and its oxidized derivatives], the emission energy could be tuned as a function of the oxidation state of the central sulfur atom.[13] Blue-green ligand-centered (^{3}LC) emission was observed when the sulfur was in the +2 ($[Ir(ppy)_2$(di(pyridin-2-yl)sulfane)$]PF_6$, with λ_{PL} = 478, 510, 548 (sh) nm, Φ_{PL} = 4% in CH_2Cl_2) or +4 oxidation states ($[Ir(ppy)_2$(2,2'-sulfinyldipyridine)$]PF_6$, with λ_{PL} = 478, 510, 548 (sh) nm, Φ_{PL} = 1% in CH_2Cl_2). Through oxidation of the sulfur atom to the +6

oxidation state ([Ir(ppy)$_2$(2,2'-sulfonyldipyridine)]PF_6, with λ_{PL} = 552 nm, Φ_{PL} = 3% in CH_2Cl_2) a red-shift and green emission of ^{3}MLCT character were observed.

Examples of nonconjugated six-membered chelate ancillary rings employing coordinating heterocycles other than pyridine include those using bis(tetrazolate),[14] bis(pyrazole)[15] or a bis-NHC (see Chart **1**).[16] In each of these examples, sky-blue emission was observed as a function of the nature of the more σ-donating heterocycle as well as the presence of the methylene bridge, with photoluminescence quantum yields in MeCN of 75%, 21% and 38%, respectively. Recently, Chi and co-workers reported a nonplanar tetradentate N^N^N^N chelate bearing a pyrazole unit and a nonconjugated tripodally-arranged terpyridine, which can coordinate to iridium forming a six-membered ring.[17] They obtained efficient, sky-blue-emitting OLEDs by using this complex as the dopant emitter. In each of these literature examples the methylene spacer disrupts the conjugation across the coordinating moieties, enabling a blue-shifted emission. The strongly donating character of the coordinating heterocycle also contributed to the blue-to-sky-blue emission of these complexes.

In an ongoing effort in the Zysman-Colman group to develop charged blue-emitting iridium(III) complexes for solution-processed OLEDs and LEECs, we investigated the coordination of the nonconjugated diimine 2,2'-(phenylmethine)dipyridine (pmdp, **L1**, Chart **2**) to iridium as an N^N ancillary ligand, in combination with either 2-(2,4-difluorophenyl)-4-mesitylpyridinato (dFmesppy) or 4-mesityl-2-phenylpyridine (mesppy) as C^N ligands, resulting in the formation of the complexes [Ir(dFmesppy)$_2$(pmdp)]PF_6, **1**, and [Ir(mesppy)$_2$(pmdp)]PF_6, **2**, respectively. The mesityl group was incorporated onto the C^N ligands to increase the solubility of the resultant complexes in organic solvents without

significantly affecting their emission energy, due to the nearly-orthogonal conformation between the mesityl substituent and the pyridine of the C^N ligands, thereby disrupting conjugation;[18] indeed, the unsubstituted ppy analog $[Ir(ppy)_2(pmdp)]Cl$ showed very poor solubility in organic solvents (such as CH_2Cl_2, $CHCl_3$, MeOH, MeCN, DMSO) and its characterization in solution was not successful. The impact of the use of the pmdp ligand is studied through comparison with two reference complexes **R1**[18a] and **R2**[19] bearing the same C^N ligands and 4,4'-di-*tert*-butyl-2,2'-bipyridine (d*t*Bubpy) as the conjugated N^N ligand. The photophysical properties of these complexes are corroborated by density functional theory (DFT) and time-dependent DFT (TD-DFT) investigations.

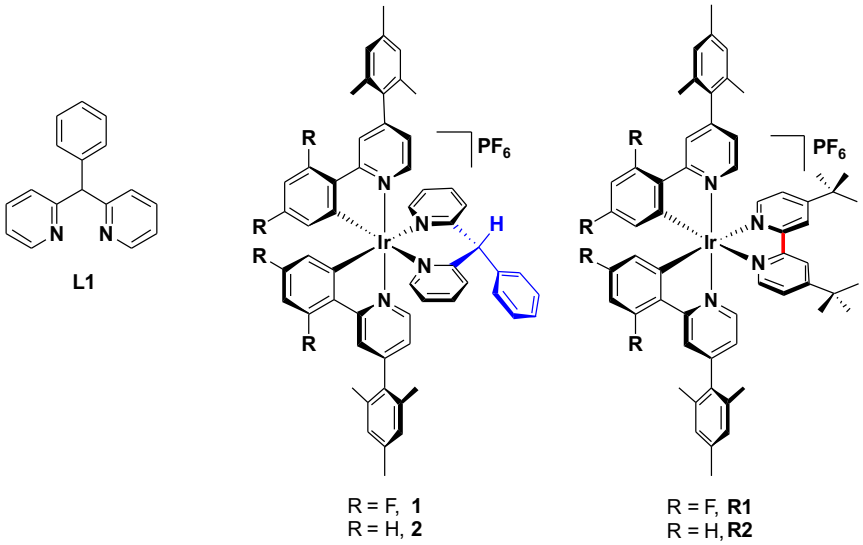

Chart **2**. Structural representation of 2,2'-(phenylmethine)dipyridine (pmdp, **L1**), used as N^N ancillary ligand in this study and complexes **1** and **2** and their reference complexes **R1**[18a] and **R2**,[19-20] respectively.

Results and Discussion

The ancillary ligand pmdp, **L1,** was obtained in 40% yield as a beige solid following a modified procedure[21] wherein 2-benzylpyridine was treated with *n*-BuLi at -78 °C and

subsequently reacted with 2-fluoropyridine under S_NAr conditions. Complexes **1** and **2** were obtained as their hexafluorophosphate salts in a two-step synthesis following our previously reported protocol.[18a] After column chromatography on silica (eluent: 0 – 8% MeOH in CH_2Cl_2) followed by an ion exchange with aqueous NH_4PF_6 and recrystallization, complexes **1** and **2** were isolated as yellow solids in excellent yields (81% and 89%, respectively) as their hexafluorophosphate salts. Solution-state NMR spectroscopy in $CDCl_3$ revealed the orientation of the phenyl ring on **L1** to be in a pseudo-axial configuration. The complexes were characterized by ^{1}H, ^{13}C and ^{31}P NMR spectroscopy and, for **1**, ^{19}F NMR spectroscopy; ESI-HR mass spectrometry, elemental analysis, and melting point determination (see Figures **S1**−**S12** in the Electronic Supporting Information, ESI†, for NMR and ESI-HR mass spectra).

Crystal Structure

Single crystals of sufficient quality of **1** were grown from vapor diffusion of a CH_2Cl_2 solution of the complex with hexane acting as the anti-solvent. The structure of **1** was determined by single-crystal X-ray diffraction (see Figure **1**, and Table **S1** in the ESI†).

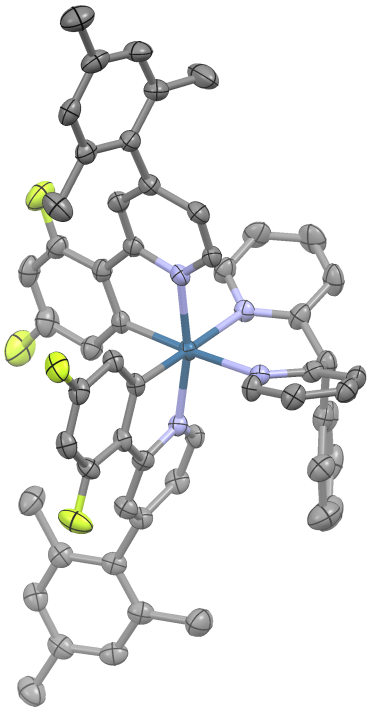

Figure **1**. Solid-state structure of complex **1**, thermal ellipsoids are drawn at the 50% probability level. Hydrogen atoms, PF_6^- counterion and solvent molecules are omitted for clarity.

Complex **1** shows a distorted octahedral coordination environment around the iridium with the two N atoms of the C^N ligands in the typical *trans* configuration. The Ir-C_{C^N} bond lengths of [2.005(4) and 2.006(4) Å] and the Ir-N_{C^N} bond lengths [2.050(4) and 2.057(4) Å] are, as expected, in the same range as the average bond lengths in **R1** [Ir-C_{C^N} = 2.000 Å and Ir-N_{C^N} = 2.035 Å]. The Ir-N_{N^N} bonds [2.197(4) and 2.201(4) Å], are notably longer than both those found in **R1** (average Ir-N_{N^N} = 2.125 Å),[18a] and those found in a related complex, $[Ir(ppy)_2(dpa)]PF_6$, where the ancillary ligand forms a nonconjugated six-membered chelate ring (average Ir-N_{N^N} = 2.171 Å).

The bite angles of the C^N ligands in **1** are 80.25(17)° and 80.47(17)°, which are in the same range as the corresponding bond angles in **R1** (average C_{C^N}-Ir-N_{C^N} = 80.8°]). The bite angle of the ancillary ligand in **1** is 87.96(13)°, which is slightly increased compared to that in $[Ir(ppy)_2(dpa)]PF_6$ [86.0(2)°].[12a] As expected, compared to the bite angle of the ancillary ligand found in **R1** [76.2(4)°], a significant enlargement can be observed. The angles between the planes of mesityl ring and the pyridine of the C^N ligands in **1** are 71.4(2)° and 78.8(2)°, which are slightly smaller than analogous inter-planar angles in **R1** [84.5° and 85.0°], while being larger than those found in the racemic form of **R2** [57.3°], but falling between the angles found in the enantiopure forms of **R2** [74.9° and 89.4°].[18a, 19]

An interesting feature revealed by the crystal structure of **1** is the geometry of the N^N ligand, which has the phenyl substituent in a pseudo-axial configuration. Additionally, the

pyridines of the ligand are affected by two conflicting preferences: that of the iridium centre for an octahedral coordination geometry, and that of the methine carbon for a tetrahedral geometry. This results in the pyridines adopting a splayed V-shape with respect to the methine [C_{py}-$C_{methine}$-C_{py} angle 117.3(4)°], the planes of the pyridine rings inclined at 39.2(2)° to each other, and angled such that the iridium centre does not sit in the same plane as either of these rings.

Electrochemical Properties

The electrochemical behavior of **1** and **2** was evaluated by cyclic voltammetry (CV) and differential pulse voltammetry (DPV) in deaerated MeCN solution at 298 K, at a scan rate of 100 mV s^{-1}, using Fc/Fc^{+} as the internal reference and referenced with respect to SCE (0.38 V vs. SCE).[22] The voltammograms are depicted in Figure **2** and the electrochemistry data are found in Table **1**.

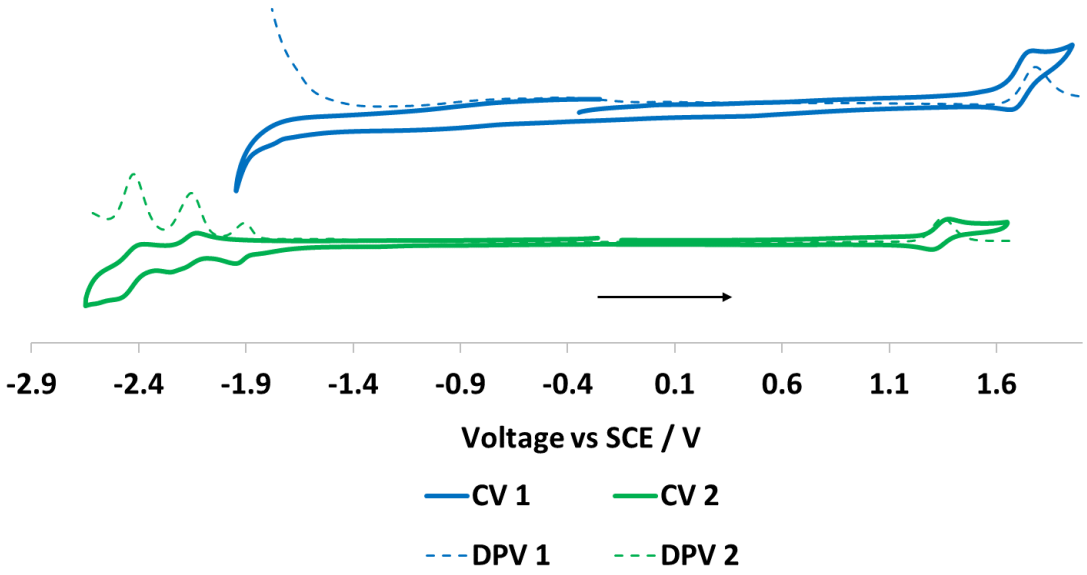

Figure **2**. Cyclic voltammetry (in solid line) and differential pulse voltammetry (in dotted line) carried out in degassed MeCN at a scan rate of 100 mV s^{-1}, referenced to SCE (Fc/Fc^+ = 0.38 V vs. SCE).[22]

Table **1**: Selected electrochemical properties of complex **1** and **2** and their reference complexes **R1** and **R2**.

	Electrochemistry[a]						
	$E_{1/2}^{ox}$ / V	ΔE_p / mV	$E_{1/2}^{red}$ / V	ΔE_p / mV	ΔE_{redox}[b] / V	E_{HOMO}[c] / eV	E_{LUMO}[c] / eV
1	1.79	80	n.d.[d]	-	n.d.[d]	-6.21	-
2	1.36	78	-1.90[e], -2.15, -2.42,	-, 120, 98	3.26	-5.78	-2.52
R1[f]	1.59	-	-1.36	-	2.95	-6.01	-3.06
R2[g]	1.17	-	-1.15[e]	-	2.32	-	-

[a] in degassed MeCN at a scan rate of 100 mV s^{-1} with Fc/Fc^+ as internal reference, and referenced with respect to SCE (Fc/Fc^+ = 0.38 V in MeCN);[22] ΔE_{redox} is the difference (V) between first oxidation and first reduction potentials; [c] $E_{HOMO/LUMO}$ = -[$E^{ox/red}$ vs Fc/Fc^+ + 4.8] eV;[23] [d] not detectable; [e] irreversible; [f] from ref. [18a]; [g] in CH_2Cl_2 from ref [20].

Both complexes exhibit a quasi-reversible single electron oxidation, which can be attributed to the Ir(III)/(IV) redox couple with contributions from the C^N ligands.[24] Complex **1**, bearing the dFmesppy C^N ligands, displays a notably more positive oxidation potential (1.79 V) than **2** (1.36 V) due to the presence of the electron-withdrawing fluorine atoms, a trend that can be also seen in the comparison of **R1** (1.59 V) and **R2** (1.17 V in CH_2Cl_2). Both **1** and **2** are more difficult to oxidize compared to their respective reference complexes **R1** and **R2**, demonstrating that the less-conjugated pmdp ligand influences less strongly the oxidation potential of the complex than the more π-accepting d*t*Bubpy ligand used in the reference complexes. Upon scanning to negative potential, surprisingly no reduction wave is observed

for complex **1**. Complex **2** exhibits three reduction waves, with the first being irreversible (-1.90 V), while the second (-2.15 V) and third (-2.42 V) being quasi-reversible. Compared to **R2** (-1.15 V in CH_2Cl_2), the first reduction wave of **2** is significantly shifted to a more negative potential (by 0.75 V), reflecting the disruption of the conjugation of the N^N ligand, making the reduction more difficult. Based on a comparison with the electrochemistry reported by Thompson *et al.*[15b] for the related complex $[Ir(tpy)_2(pz_3CH)]CF_3SO_3$ [where tpy is 2-*para*-tolylpyridinato and pz_3CH is η^2–tri(1*H*-pyrazol-3-yl)methane], the first two reduction waves are the result of successive reductions of the pyridyl rings of the two C^N ligands while the third reduction wave corresponds to the reduction of the ancillary ligand.

Photophysical Properties

To study the impact of the interruption of the electronic communication between the pyridine rings within the ancillary ligand **L1**, we investigated the photophysical properties of **1** and **2**. UV-vis absorption spectra for **1** and **2** are shown in Figure **3** with the data summarized in Table **S2** in the ESI†.

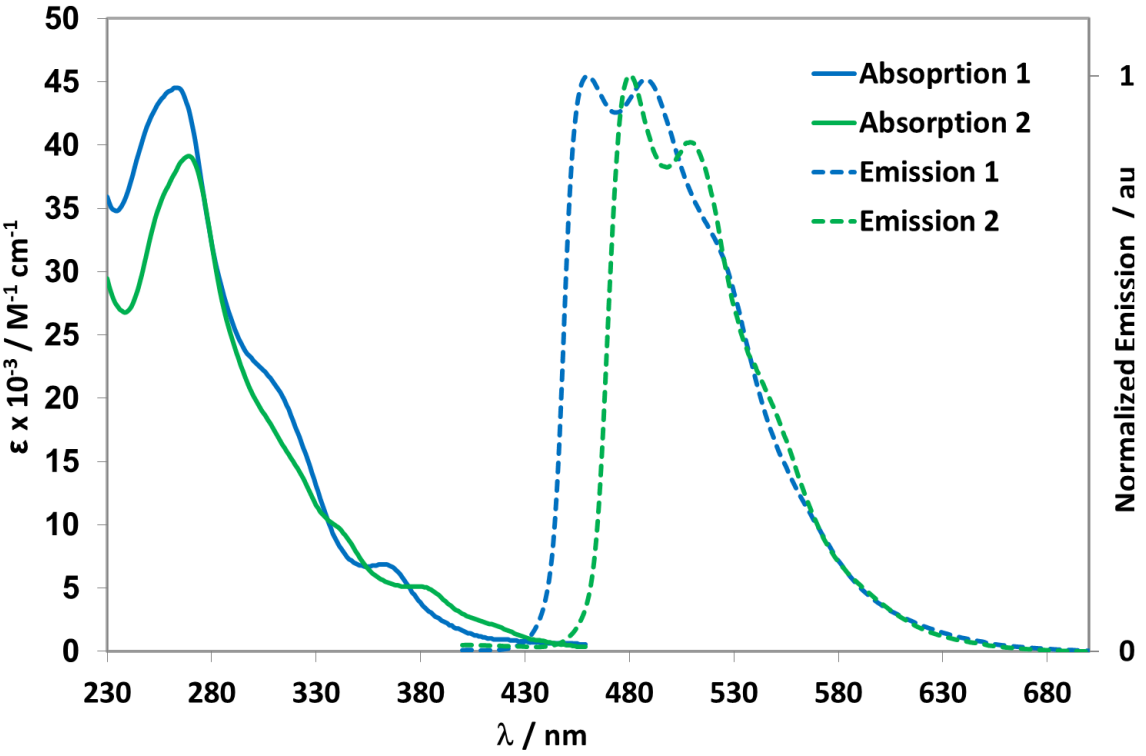

Figure **3**. UV-vis absorption and photoluminescence spectra of **1** and **2** in MeCN at 298 K.

Complexes **1** and **2** both exhibit similar absorption profiles to their respective reference complexes **R1** and **R2**. High intensity bands below 270 nm (ε on the order of 39 – 45 × 10^3 $M^{-1}cm^{-1}$) are observed for **1** and **2** and are assigned as ligand-centered π–π* transitions, which is a typical feature for associated complexes of the form of $[Ir(C^N)_2(N^N)]^+$.[25] Moderately intense bands (ε on the order of 9 – 20 × 10^3 $M^{-1}cm^{-1}$) in the region of 310 – 345 nm are assigned to a combination of spin-allowed singlet metal-to-ligand and ligand-to-ligand charger transfer (^{1}MLCT/^{1}LLCT) transitions, and appear as a shoulder. These are blue-shifted by 31 nm (2879 cm^{-1}) for **1** compared to **2**, due to the electron-withdrawing fluorine atoms present in the former. At lower energies both complexes exhibit low intensity bands (ε on the order of 0.5 – 6 × 10^{-3} $M^{-1}cm^{-1}$) in the region of 360-450 nm that are attributed to a combination of spin-forbidden ^{3}MLCT/^{3}LLCT transitions. These assignments are corroborated by theory (*vide infra*).

The photoluminescence properties of **1** and **2** were investigated at 298 K in degassed MeCN (Figure **3**), as polymethyl methacrylate (PMMA) doped films (5 wt% of complex in PMMA) and as spin-coated neat films (Figure **4a**). The spectra of **1** and **2** in a 2-methyltetrahydrofuran (2-MeTHF) glass at 77 K are depicted in Figure **4b**. The photophysical data of **1** and **2** and **R1** and **R2** are summarized in Table **2**.

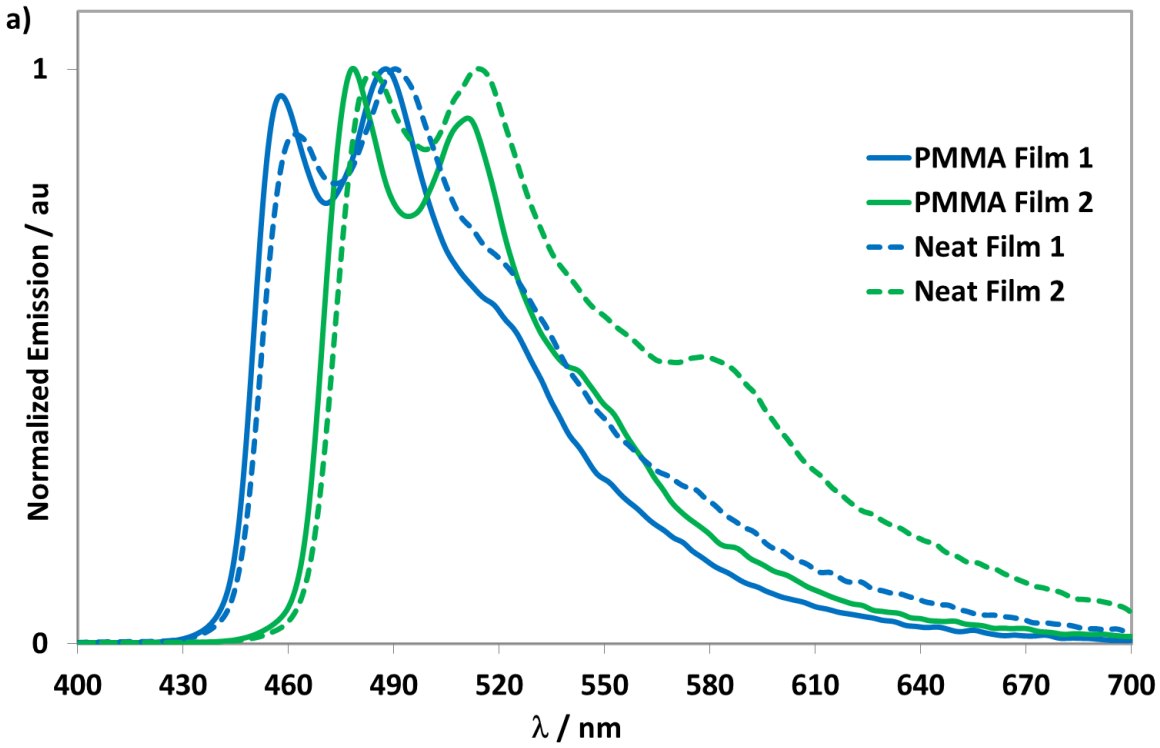

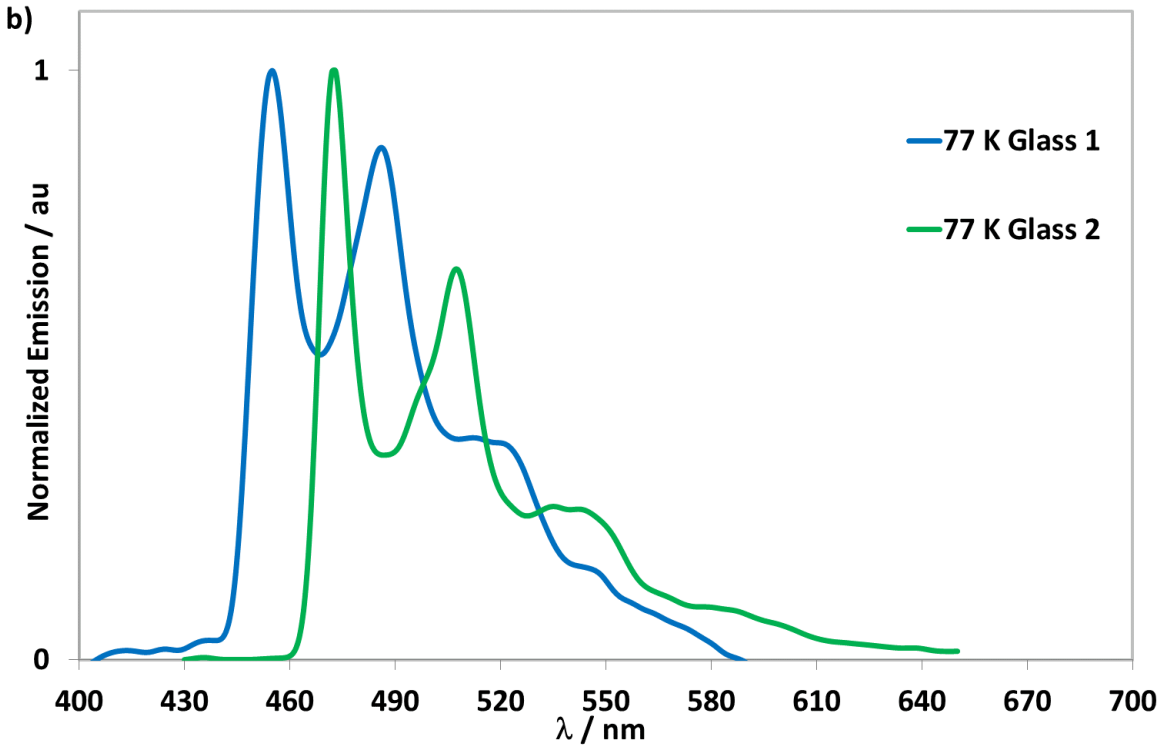

Figure **4**. a) Photoluminescence spectra of **1** and **2** recorded in PMMA doped films (5 wt% of complex in PMMA) in solid lines and in neat film (spin-coated from 2-methoxyethanol) in dotted lines (λ_{exc} = 360 nm); b) Photoluminescence spectra of complexes **1** and **2** recorded in 2-MeTHF glass at 77 K (λ_{exc} = 360 nm).

Table **2**. Photophysical properties of **1** and **2** and their reference complexes **R1** and **R2**.

	MeCN[a]			**PMMA Film**[b]			**Neat Film**[c]			**Glass**[d]	
	λ_{PL}[e] / nm	Φ_{PL}[f] / %	τ_{PL}[g] / ns	λ_{PL}[e] / nm	Φ_{PL}[h] / %	τ_{PL}[g] / ns	λ_{PL}[e] / nm	Φ_{PL}[h] / %	τ_{PL}[g] / ns	λ_{PL}[e] / nm	τ_{PL}[g] / ns
1	460, 488	30	186 (15%) 445 (85%)	459, 488	46	325 (5%) 1260 (35%) 3260 (60%)	464, 490, 527	21	75 (12%) 263 (46%) 755 (42%)	455, 487, 516	20 (1%) 2920 (99%)

2	481, 509	11	95 (16%) 206 (84%)	478, 512	26	162 (4%) 770 (31%) 2000 (65%)	485, 514, 581	9	71 (33%) 210 (63%) 1195 (4%)	473, 508, 539 ,	200 (1%) 2800 (99%)
R1[i]	515	80	1370	474, 502	97	16300	508	54	390 (68%) 1230 (34%)	-	-
R2[j]	577	40	757	-	-	-	478, 516, 550	18	25 (6%) 211 (42%) 672 (52%)	-	-

[a] In deaerated MeCN at 298 K; [b] at 298 K, spin-coated from a 2-methoxyethanol solution of 5 wt% of the complex in PMMA on a pristine quartz substrate; [c] at 298 K, spin-coated from a 2-methoxyethanol solution; [d] in 2-MeTHF at 77 K; [e] λ_{exc} = 360 nm; [f] Quinine sulfate used as the reference (Φ_{PL} = 54.6% in 0.5 M H_2SO_4 at 298 K);[26] [g] λ_{exc} = 378 nm; [h] Measured using an integrating sphere; [i] from ref. [18a]; [j] in CH_2Cl_2 from ref [19-20].

Upon photoexcitation at 360 nm in MeCN, **1** and **2** show structured emission profiles, indicative of an emission with a significant ligand-centered character (see below for spin densities), with maxima at 460 and 480 nm for **1**, and 481 and 509 nm for **2**, the former being more intense in both cases. The emission maxima of **1** is blue-shifted by 55 nm (2322 cm^{-1}) compared to that of **R1** (λ_{PL} = 515 nm),[18a] which itself presents an unstructured mixed charge-transfer emission profile. The same trend is observed when comparing the emission of **2** to **R2** (λ_{PL} = 577 nm in CH_2Cl_2).[19-20] Comparison of the photophysical properties of **2** with the archetype complex $[Ir(ppy)_2(bpy)]PF_6$ (λ_{PL} = 602 nm, Φ_{PL} = 9%) reveals an even more pronounced blue-shift (Δ = 121 nm, 4179 cm^{-1}).[11] A comparison with the structurally related complex $[Ir(ppy)_2(dpyOH\text{-}H)]Cl$ (with λ_{PL} = 477, 507 nm, Φ_{PL} = 10% in MeCN) reveals an essentially similar photophysical profile.[10] A final comparison of the MeCN emission profiles of **1** with $[Ir(dFppy)_2(o\text{-xylbiim})]PF_6$ (where *o*-xylbiim = 1,1′-(α,α′-*o*-xylylene)-2,2′-biimidazole) reveals that both complexes show a similar LC emission with the maximum of

the latter at 459 nm, but with a Φ_{PL} of 90%. Therefore, the magnitude of the effect of breaking the conjugation in the N^N ligand is similar to the use of one of the most electron-donating ancillary ligands.[18a]

The photoluminescence quantum yield ($\Phi_{PL,MeCN}$) of **1** is 30%, which is notably higher than that of **2** ($\Phi_{PL,MeCN}$ = 11%), a trend also observed in **R1** and **R2**. Compared to their reference complexes **R1** (Φ_{PL} = 80%) and **R2** (Φ_{PL} = 40%), **1** and **2** show much lower Φ_{PL} values, which can be rationalized by the flexibility of the N^N ancillary ligand leading to an increased non-radiative decay pathway. Both complexes exhibit bi-exponential emission lifetimes, τ_{PL}, in the sub-microsecond regime.

The emission energies and profiles of **1** and **2** in 5 wt% PMMA-doped films are not significantly changed compared to those in MeCN. The photoluminescence quantum yields of the PMMA-films are increased ($\Phi_{PL,PMMA}$ = 46 and 26% for **1** and **2**, respectively) compared to the solution-state measurements. This behavior is also observed in **R1** and is mainly attributed to a reduction in k_{nr} due to the expected reduction of the conformational motions of both the mesityl groups, and in the case of **1**, the N^N ligand. Both complexes exhibit a three-component emission decay in the sub-microsecond regime in doped films, with the longest component significantly longer than the corresponding long component of τ_{PL} in MeCN. In spin-coated neat films the structured emission profiles are likewise not significantly changed compared from those in MeCN; however, they exhibit a more pronounced shoulder at 527 and 581 nm, respectively. Compared to the neat films, the PMMA-doped films show a slight blue-shift [$\lambda_{PL,PMMA}$ = 459 (sh), 488 nm and $\lambda_{PL,PMMA}$ = 478, 512 (sh) nm for **1** and **2**, respectively]. The photoluminescence quantum yields of the neat films ($\Phi_{PL,\ Neat}$) are lower ($\Phi_{PL,Neat}$ = 21

and 9% for **1** and **2**, respectively) than those seen in the solution-state measurements. The decrease in Φ_{PL} in neat films was also observed in **R1** and **R2** and can be explained by π-stacking intermolecular interactions between mesityl rings on adjacent complexes, providing an avenue for aggregation-caused quenching. Both complexes exhibit a three-component emission decay in the sub-microsecond regime in neat films, significantly shorter than in doped PMMA films. There is no significant shifting in the emission energy at low temperature compared to measurements at 298 K, reflecting that the emission remains ligand-centered under both sets of conditions. The emission decay profiles for both **1** and **2** are biexponential in the glass, with an expected much longer emission lifetime compared to those in MeCN.

Theoretical calculations

To gain more insights into the nature of the excited-states in both **1** and **2**, we have performed DFT and TD-DFT calculations in acetonitrile (see the ESI† for details). First, for **1** the DFT optimized geometry present Ir-C_{C^N}, Ir-N_{C^N} and Ir-N_{N^N} bond lengths of 2.003 and 2.003 Å, 2.058 and 2.065 Å, and 2.223 and 2.242 Å, respectively. These values are close to the ones obtained in the crystal (*vide supra*) with a mean absolute deviation of 0.018 Å. The bite angles are 80.2° and 80.5° for the C^N ligands, and 86.9° for the ancillary ligand, are likewise close to their experimental counterparts. This indicates that the selected theoretical protocol is physically sound for the considered complexes. The DFT calculations indicate that when going from **1** to **2**, the energy of the HOMO increases by 0.34 eV, which is rather consistent with the electrochemical value (0.43 eV, see Table 1), whereas the energy of the LUMO is shifted to higher energy by 0.11 eV, resulting in a HOMO-LUMO gap that is smaller by 0.23 eV in the fluorine-free complex. As can be seen in Figure **5**, the HOMO is mainly centered on the metal and the cyclometalating aryl rings of the C^N ligands, whereas

the LUMO is principally localized on the pyridyl rings of the C^N ligand that is the furthest away from the ancillary phenyl ring. This holds for both compounds, so that the observed electrochemical differences are mainly due to the inductive effects of the fluorine atoms and not to a change in shape of the frontier orbitals. These MO topologies are also consistent with the fact that the energy of the HOMO significantly varies from **1** to **2**, whereas the LUMO energy is less affected.

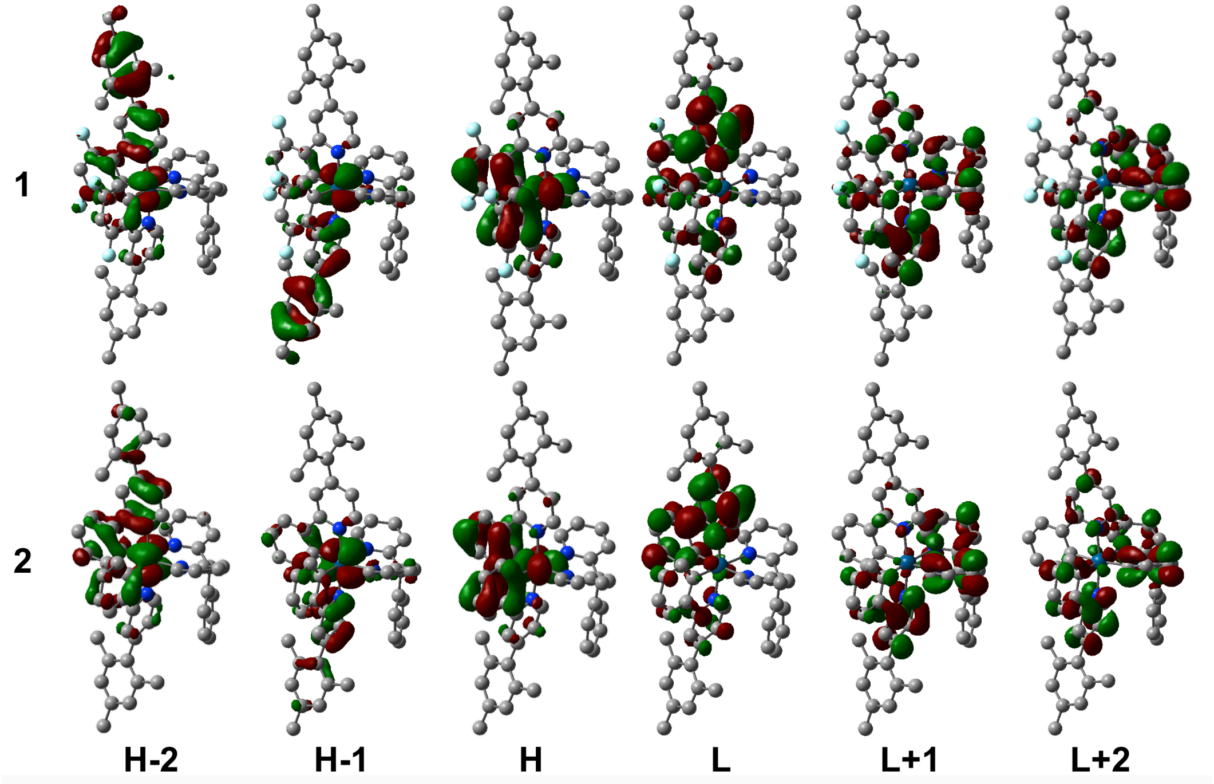

Figure **5**. Representation of the six frontier orbitals of **1** (top) and **2** (bottom). A contour threshold of 0.03 au is used, and the hydrogen atoms have been omitted for clarity.

TD-DFT calculations return several low-lying triplet states, the lowest being located at 442 nm in **1** and 463 nm in **2.** The lowest dipole-allowed singlet excited states are computed at 373 nm (f=0.054) in **1** and 399 nm (f=0.063) in **2**, corresponding to a blue-shift of 26 nm between the two complexes, in line of the experimental value (31 nm, *vide supra*) though the computed wavelengths are slightly larger than their experimental counterparts. These singlet

transitions are mainly ascribable to a HOMO-LUMO electronic promotion, and therefore present a mixed ^{1}MLCT/^{1}LLCT character, L being the C^N ligand(s).; the N^N ligand not being involved in this transition. In **1**, the next singlet transitions presenting significant oscillator strengths are located at 340 nm (f=0.012), 337 nm (f=0.025) and 329 nm (f=0.202). These three absorptions mainly correspond to HOMO-1 to LUMO+1, HOMO-2 to LUMO and HOMO-2 to LUMO+1 electronic transitions, indicating that the first and the third present a significant CT character towards the N^N ligand.

In **1**, the DFT computed 0-0 phosphorescence wavelength is 476 nm, a value that takes into account the zero-point vibrational effects. In **2**, the computed value is 501 nm, at lower energy in agreement with experimental data. In both **1** and **2**, the spin density plot of the lowest triplet excited-state shows contributions from the metal and C^N ligand residing the closest to the phenyl ring of the ancillary ligand, confirming the mixed nature of the emitting state (Figure **6**). We would therefore make the hypothesis that the interaction with the phenyl ring of the ancillary ligand tends to stabilize the spin density on the closest C^N ligand. Indeed, for **2**, we have been able to locate a triplet state presenting a more uniform delocalization of its density on both C^N ligands, but it is higher in energy than the one represented in Figure **6.**

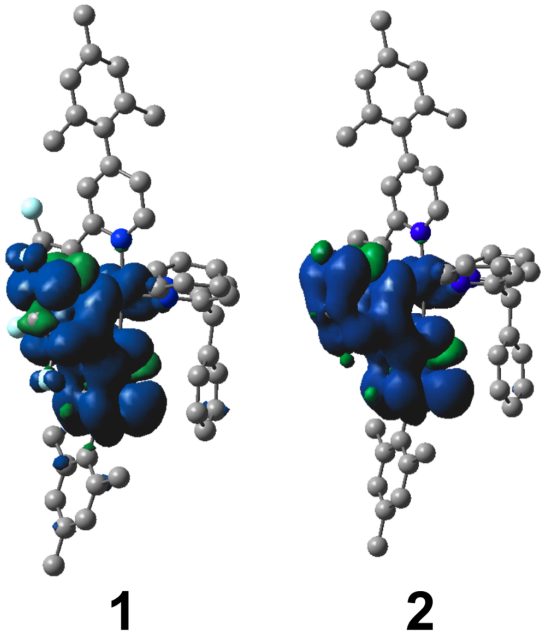

Figure **6**. Representation of the spin density difference plot for **1** (left) and **2** (right). Contour threshold: 0.0008 au.

Conclusions

Two new cationic blue and blue-green-emitting iridium complexes of the form $[Ir(C^N)_2(N^N)]PF_6$ bearing mesitylated C^N ligands and a six-membered chelate methine bridged N^N are reported. The ancillary ligand **L1** (pmdp = 2,2'-(phenylmethine)dipyridine) consists of two pyridyl rings, whose electronic crosstalk is disrupted by a phenyl substituted methylene group. For both complexes we performed the synthesis, characterization and optoelectronic properties. The crystal structure of **1** reveals that the phenyl substituent on the ancillary ligand adopts a pseudo-axial configuration. We have shown that by using such an ancillary ligand a significant blue-shift in the emission is observed for **1** and **2** compared to their reference complexes **R1** and **R2**. The photoluminescence quantum yields were lower compared to the reference complexes as a consequence of the increased fluxional motion of the ancillary ligand. Photoluminescence studies were also performed in neat films and the

PMMA-doped films showing similar structured emission profiles. We have demonstrated that employing the nonconjugated N^N ligand 2,2'-(phenylmethine)dipyridine, **L1** is a successful strategy to blue-shift the emission of Ir(III) complexes.

Acknowledgment

We thank Umicore AG for the gift of materials. We thank the EPSRC UK National Mass Spectrometry Facility at Swansea University for analytical services. C.H. acknowledges the *Région Bretagne*, France for funding. D.J. acknowledges the European Research Council and the *Région des Pays de la Loire* for financial support in the framework of a Starting Grant (Marches - 278845) and the LUMOMAT RFI project, respectively. This research used resources of 1) the GENCI-CINES/IDRIS, 2) the CCIPL (C*entre de Calcul Intensif des Pays de Loire*), 3) a local Troy cluster. E.Z.-C. acknowledges the University of St Andrews and EPSRC (EP/M02105X/1) for financial support.

Supporting information. NMR and mass spectra for **L1** and **1-2**, Supplementary crystallographic, electrochemical and photophysical data, description of the computational protocol and results. CIF file for the X-ray structure of **1** (CCDC: 1821381).

References

(1). (a) K. P. S. Zanoni, R. L. Coppo, R. C. Amaral and N. Y. Murakami Iha, *Dalton Trans.*, 2015, **44**, 14559-14573; (b) A. F. Henwood and E. Zysman-Colman, *Chem. Commun.*, 2017, **53**, 807-826; (c) C. W. Lu, Y. Wang and Y. Chi, *Chemistry*, 2016, **22**, 17892-17908.
(2). (a) H. Xu, R. Chen, Q. Sun, W. Lai, Q. Su, W. Huang and X. Liu, *Chem. Soc. Rev.*, 2014, **43**, 3259-3302; (b) C. Bizzarri, F. Hundemer, J. Busch and S. Bräse, *Polyhedron*, 2018, **140**, 51-66.
(3). (a) A. F. Henwood and E. Zysman-Colman, *Top. Curr. Chem.*, 2016, **374**, 36; (b) A. F. Henwood and E. Zysman-Colman, in *Iridium(III) in Optoelectronic and Photonics Applications*, John Wiley & Sons, Ltd, 2017, pp. 275-357; (c) For recent reviews on LEECs see: R. D. Costa, E. Ortí, H. J. Bolink, F. Monti, G. Accorsi and N. Armaroli, *Angew. Chem. Int. Ed.*, 2012, **51**, 8178-8211. ; (d) S. B. Meier, D. Tordera, A. Pertegás, C. Roldán-Carmona, E. Ortí and H. J. Bolink, *Mater. Today*, 2014, **17**, 217-223.
(4). (a) J.-H. Jou, S. Kumar, A. Agrawal, T.-H. Li and S. Sahoo, *J. Mater. Chem. C*, 2015, **3**, 2974-3002; (b) X. Yang, X. Xu and G. Zhou, *J. Mater. Chem. C*, 2015, **3**, 913-944.

(5). (a) H.-C. Li, P.-T. Chou, Y.-H. Hu, Y.-M. Cheng and R.-S. Liu, *Organometallics*, 2005, **24**, 1329-1335; (b) R. Zhu, J. Lin, G.-A. Wen, S.-J. Liu, J.-H. Wan, J.-C. Feng, Q.-L. Fan, G.-Y. Zhong, W. Wei and W. Huang, *Chem. Lett.*, 2005, **34**, 1668-1669; (c) V. Thamilarasan, A. Jayamani, P. Manisankar, Y.-I. Kim and N. Sengottuvelan, *Inorg. Chim. Acta*, 2013, **408**, 240-245.
(6). (a) Y. H. Song, Y. C. Chiu, Y. Chi, Y. M. Cheng, C. H. Lai, P. T. Chou, K. T. Wong, M. H. Tsai and C. C. Wu, *Chem. Eur. J.*, 2008, **14**, 5423-5434; (b) C.-F. Chang, Y.-M. Cheng, Y. Chi, Y.-C. Chiu, C.-C. Lin, G.-H. Lee, P.-T. Chou, C.-C. Chen, C.-H. Chang and C.-C. Wu, *Angew. Chem. Int. Ed.*, 2008, **47**, 4542-4545; (c) F. Zhang, D. Ma, L. Duan, J. Qiao, G. Dong, L. Wang and Y. Qiu, *Inorg Chem*, 2014, **53**, 6596-6606.
(7). C. Hierlinger, T. Roisnel, D. B. Cordes, A. M. Z. Slawin, D. Jacquemin, V. Guerchais and E. Zysman-Colman, *Inorg Chem*, 2017, **56**, 5182-5188.
(8). C. Hierlinger, A. K. Pal, F. Stella, T. Lebl, D. B. Cordes, A. M. Z. Slawin, D. Jacquemin, V. Guerchais and E. Zysman-Colman, *Inorg Chem*, 2018, **ASAP**, DOI: 10.1021/acs.inorgchem.1027b02940
(9). E. Sauvageot, P. Lafite, E. Duverger, R. Marion, M. Hamel, S. Gaillard, J.-L. Renaud and R. Daniellou, *J. Organomet. Chem.*, 2016, **808**, 122-127.
(10). G. Volpi, C. Garino, E. Breuza, R. Gobetto and C. Nervi, *Dalton Trans.*, 2012, **41**, 1065-1073.
(11). For examples see: S. Ladouceur, D. Fortin and E. Zysman-Colman, *Inorg. Chem.*, 2011, **50**, 11514-11526.
(12). (a) M. C. Tseng, W. L. Su, Y. C. Yu, S. P. Wang and W. L. Huang, *Inorg. Chim. Acta*, 2006, **359**, 4144-4148; (b) W.-T. Chen, Y.-J. Chen, C.-S. Wu, J.-J. Lin, W.-L. Su, S.-H. Chen and S.-P. Wang, *Inorg. Chim. Acta*, 2013, **408**, 225-229; (c) F. Sguerra, R. Marion, G. H. V. Bertrand, R. Coulon, É. Sauvageot, R. Daniellou, J. L. Renaud, S. Gaillard and M. Hamel, *J. Mater. Chem. C*, 2014, **2**; (d) E. Sauvageot, R. Marion, F. Sguerra, A. Grimault, R. Daniellou, M. Hamel, S. Gaillard and J.-L. Renaud, *Organic Chemistry Frontiers*, 2014, **1**.
(13). C. M. Brown, M. J. Kitt, Z. Xu, D. Hean, M. B. Ezhova and M. O. Wolf, *Inorg Chem*, 2017, **56**, 15110-15118.
(14). (a) E. Matteucci, A. Baschieri, A. Mazzanti, L. Sambri, J. Avila, A. Pertegas, H. J. Bolink, F. Monti, E. Leoni and N. Armaroli, *Inorg Chem*, 2017, **56**, 10584-10595; (b) A. Baschieri, F. Monti, E. Matteucci, A. Mazzanti, A. Barbieri, N. Armaroli and L. Sambri, *Inorg Chem*, 2016, **55**, 7912-7919.
(15). (a) S. Meng, I. Jung, J. Feng, R. Scopelliti, D. Di Censo, M. Grätzel, M. K. Nazeeruddin and E. Baranoff, *Eur. J. Inorg. Chem.*, 2012, **2012**, 3209-3215; (b) J. Li, P. I. Djurovich, B. D. Alleyne, M. Yousufuddin, N. N. Ho, J. C. Thomas, J. C. Peters, R. Bau and M. E. Thompson, *Inorg. Chem.*, 2005, **44**, 1713-1727.
(16). (a) C.-H. Yang, J. Beltran, V. Lemaur, J. Cornil, D. Hartmann, W. Sarfert, R. Fröhlich, C. Bizzarri and L. De Cola, *Inorg. Chem.*, 2010, **49**, 9891-9901; (b) S. B. Meier, W. Sarfert, J. M. Junquera-Hernández, M. Delgado, D. Tordera, E. Ortí, H. J. Bolink, F. Kessler, R. Scopelliti, M. Grätzel, M. K. Nazeeruddin and E. Baranoff, *J. Mater. Chem. C*, 2013, **1**, 58; (c) F. Monti, F. Kessler, M. Delgado, J. Frey, F. Bazzanini, G. Accorsi, N. Armaroli, H. J. Bolink, E. Orti, R. Scopelliti, M. K. Nazeeruddin and E. Baranoff, *Inorg Chem*, 2013, **52**, 10292-10305; (d) L. He, Z. Wang, L. Duan, C. Yang, R. Tang, X. Song and C. Pan, *Dalton Trans*, 2016, **45**, 5604-5613; (e) C. Yang, F. Mehmood, T. L. Lam, S. L.-F. Chan, Y. Wu, C.-S. Yeung, X. Guan, K. Li, C. Y.-S. Chung, C.-Y. Zhou, T. Zou and C.-M. Che, *Chem. Sci.*, 2016, **7**, 3123-3136; (f) J. Jin, H.-W. Shin, J. H. Park, J. H. Park, E. Kim, T. K. Ahn, D. H. Ryu and S. U. Son, *Organometallics*, 2013, **32**, 3954-3959.
(17). Y. S. Li, J. L. Liao, K. T. Lin, W. Y. Hung, S. H. Liu, G. H. Lee, P. T. Chou and Y. Chi, *Inorg Chem*, 2017, **56**, 10054-10060.

(18). (a) A. F. Henwood, A. K. Bansal, D. B. Cordes, A. M. Z. Slawin, I. D. W. Samuel and E. Zysman-Colman, *J. Mater. Chem. C*, 2016, **4**, 3726-3737; (b) D. Rota Martir, A. K. Bansal, V. Di Mascio, D. B. Cordes, A. F. Henwood, A. M. Z. Slawin, P. C. J. Kamer, L. Martinez-Sarti, A. Pertegas, H. J. Bolink, I. D. W. Samuel and E. Zysman-Colman, *Inorganic Chemistry Frontiers*, 2016, **3**, 218-235; (c) V. N. Kozhevnikov, Y. Zheng, M. Clough, H. A. Al-Attar, G. C. Griffiths, K. Abdullah, S. Raisys, V. Jankus, M. R. Bryce and A. P. Monkman, *Chem. Mater.*, 2013, **25**, 2352-2358.
(19). D. R. Martir, C. Momblona, A. Pertegás, D. B. Cordes, A. M. Z. Slawin, H. J. Bolink and E. Zysman-Colman, *ACS Applied Materials & Interfaces*, 2016, **8**, 33907-33915.
(20). D. Rota Martir, G. J. Hedley, D. B. Cordes, A. M. Z. Slawin, D. Escudero, D. Jacquemin, T. Kosikova, D. Philp, D. M. Dawson, S. E. Ashbrook, I. D. W. Samuel and E. Zysman-Colman, *Dalton Trans.*, 2016, **45**, 17195-17205.
(21). A. Santoro, C. Sambiagio, P. C. McGowan and M. A. Halcrow, *Dalton Trans*, 2015, **44**, 1060-1069.
(22). V. V. Pavlishchuk and A. W. Addison, *Inorg. Chim. Acta*, 2000, **298**, 97-102.
(23). C. M. Cardona, W. Li, A. E. Kaifer, D. Stockdale and G. C. Bazan, *Adv. Mater.*, 2011, **23**, 2367-2371.
(24). S. Ladouceur and E. Zysman-Colman, *Eur. J. Inorg. Chem.*, 2013, **2013**, 2985-3007.
(25). L. Flamigni, A. Barbieri, C. Sabatini, B. Ventura and F. Barigelletti, *Top. Curr. Chem.*, 2007, **281**, 143-203.
(26). W. H. Melhuish, *J. Phys. Chem.*, 1961, **65**, 229-235.

TOC

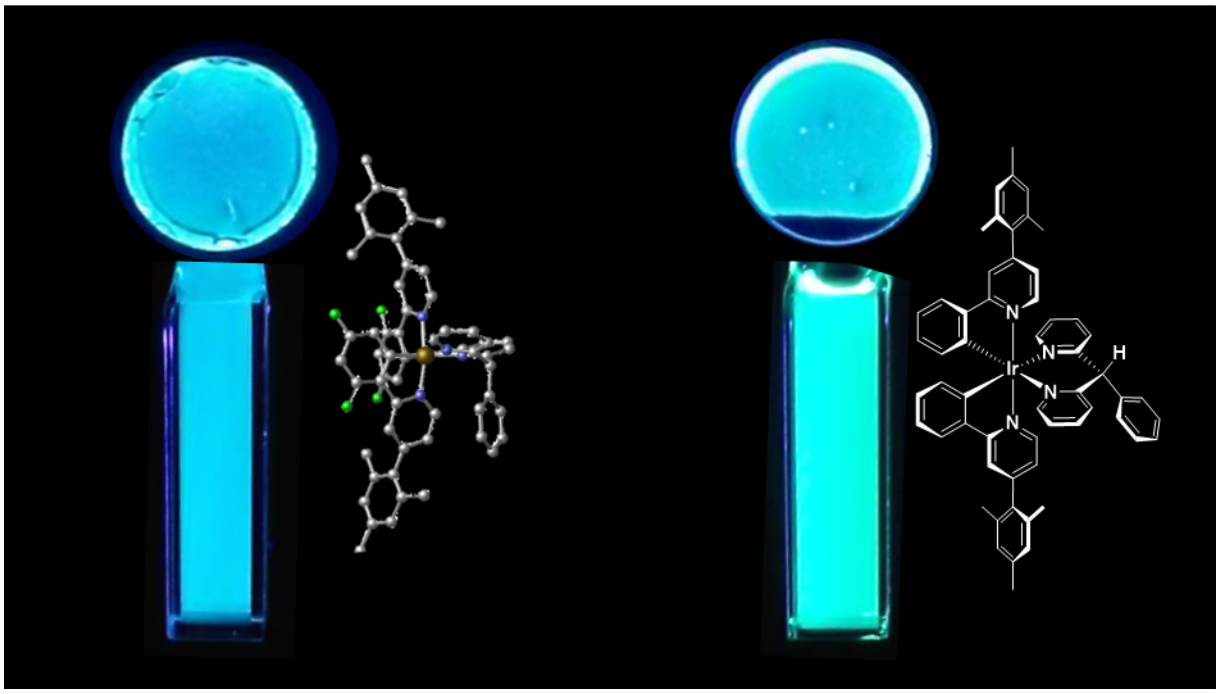

Synopsis

Blue and blue-green- emitting cationic Ir(III) complexes bearing mesitylated C^N ligands and a nonconjugated N^N ligand have been studied, and the properties of these complexes contrasted to reference complexes bearing a conjugated N^N ligand to elucidate the impact of both the chelate ring size and the breaking of conjugation in the ancillary ligand on the optoelectronic properties of the complex.